AIP | Physics of Fluids

Influence of high-frequency vibration on the Rayleigh–Marangoni instability in a two-layer system

Qiusheng Liu and Rong Liu

Citation: Phys. Fluids **23**, 034105 (2011); doi: 10.1063/1.3554765
View online: http://dx.doi.org/10.1063/1.3554765
View Table of Contents: http://pof.aip.org/resource/1/PHFLE6/v23/i3
Published by the American Institute of Physics.

Influence of high-frequency vibration on the Rayleigh–Marangoni instability in a two-layer system

Qiusheng Liu and Rong Liu[a)]
National Microgravity Laboratory, Institute of Mechanics, Chinese Academy of Sciences, Beijing 100190, China

(Received 28 March 2010; accepted 20 January 2011; published online 22 March 2011)

The influences of high-frequency vibrations on the Rayleigh–Marangoni instability in a two-layer system are investigated theoretically in the framework of the averaging method. We focus on the effects of vertical and horizontal vibrations on the stability of different convection modes. The results show that vertical vibrations significantly stabilize the system, while horizontal vibrations significantly destabilize it. In the presence of vertical vibrations, instability only occurs in a system heated from below. However, in the presence of horizontal vibrations, instability can also occur in a system cooled from below. When Marangoni effect is dominant at the interface, it is found that there are four types of coupling modes. The oscillatory convection is the result of the competition between different modes. In the presence of Marangoni effect at the interface, the structure of the interfacial flow is complicated. In some cases, small counter-rolls may develop to preserve the nonslip condition of fluids in either the upper layer or the lower layer. © *2011 American Institute of Physics*. [doi:10.1063/1.3554765]

I. INTRODUCTION

Oscillatory motion in liquid layers has been known as an effective way to enhance the performance of many applications. The related problems of oscillatory convection in a two-layer system have received significant attention because of its technological importance.

The mechanisms of oscillatory instabilities in a two-layer or multilayer system are complicated. In contrast to the Rayleigh–Bénard problem for a one-layer system, the linearized controlling equations for a two-layer system are not self-adjoint such that oscillatory instability is possible, in general. More physical mechanisms of the instabilities in a two-layer system can be referred in many previous works.[1–8] In the absence of vibration and Marangoni effect, there are two different cases where oscillatory instabilities have been predicted. The first case is that the densities of fluids are close to each other so that the deviations of the densities with respect to temperature are comparable with the density difference of the reference state, and the oscillation may be self-sustained as interfacial waves. This kind of oscillatory convection has been studied in Refs. 1, 2, and 5. The second case is that the oscillation is driven by hydrodynamic and thermal interaction at the interface. Rasenat *et al.*[3] showed that an oscillatory Rayleigh convection could develop, involving no interfacial deformation. However, the critical Rayleigh number is given by the nonoscillatory branch, so oscillatory Rayleigh instability is difficult or sometimes impossible to be observed in experiments at the onset of convection.

In many situations, both surface tension and buoyancy play important roles in driving convection in liquid layers. For Rayleigh–Bénard problems, both instability analysis and experimental observation have found two possible modes of convection: thermal coupling mode and mechanical coupling mode. For a two-layer system heated from below, the thermal coupling mode is characterized by rolls in each layer rotating in the opposite directions, while the mechanical coupling mode is characterized by rolls rotating in the same direction. Liu and Zhou[7,8] investigated the Rayleigh–Marangoni–Bénard convection in a two-layer system consisting of silicon oil 10cs and fluorinert FC70. It was shown that oscillatory Rayleigh–Marangoni–Bénard convection may occur in a narrow gap of $1.461 \leq h \leq 1.564$ for the Bond number, $\mathrm{Bo}=15.35$, in which h is the ratio between the depths of the upper liquid and the lower liquid.

Vibrations as well as gravitation and surface tension are known to be an effective way to affect the behaviors of convection in fluid systems. Gershuni and Lyubimov[9] firstly used the averaging method to describe the "thermal vibrational convection" in the limit of high-frequency and small amplitude. In Ref. 9, the term thermal vibrational convection is used by the authors in two ways. The first one is connected with the vibrational effects on convection, heat, and mass transfer caused by static gravity field. The second one is proposed to refer to the specific regular flows that appear under vibration in a cavity filled with a fluid. The effects of vibration on the onset of convection in a two-layer system has been investigated in the framework of averaging method by some authors.[9–11] The physics of the Rayleigh–Marangoni instability has been extensively investigated. However, to our knowledge, investigations devoted to the influence of vibration on the oscillatory gap of the depth ratio are very limited. Motivated by the previous works, we have made a tentative study of the influences of vibrations on the oscillatory Rayleigh–Marangoni convection. The present paper is only devoted to the case of high-frequency vibrations, i.e., the period of vibration is much smaller than the reference hydro-

[a)]Electronic mail: liurong@imech.ac.cn.

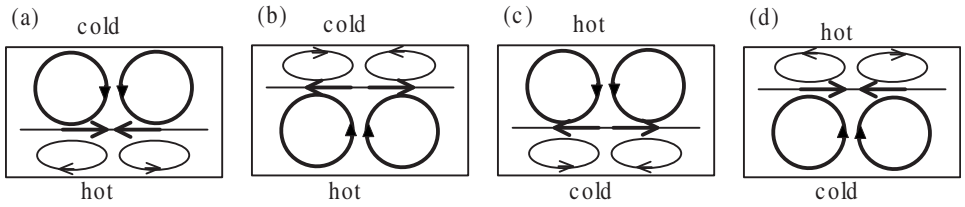

FIG. 1. Schematic of four different types of surface-driven flow in a two-layer system: (a) convection initiating in the upper fluid when heated from below, (b) convection initiating in the lower fluid when heated from below, (c) convection initiating in the upper fluid when cooled from below, and (d) convection initiating in the lower fluid when cooled from below.

dynamic time and the amplitude of vibration is much smaller than the reference length. In this case, the averaging method can be safely applied to study the effects of vibrations.

Our paper is organized as follows. In Sec. II, the mathematical formulation of the problem is presented based on the averaging method. In Sec. III, the numerical method is described briefly. In Sec. IV, the influences of vertical and horizontal vibrations on the Rayleigh–Marangoni instability are studied. Finally, conclusions are given in Sec. V.

II. MATHEMATICAL MODEL

We consider two-dimensional thermal convection under high-frequency vibrations in a two-layer system. The physical model, depicted in Fig. 1, consists of a fluid of depth d_2 underlying another fluid of depth d_1 (see also Fig. 2). The total depth of the combined layers d is defined as $d=d_1+d_2$. The combined layers are infinite in the horizontal directions. The upper and lower boundaries are rigid walls maintained at constant temperatures. The surface tension σ is assumed to be a linear function of temperature T, i.e., $\sigma=\sigma_0-\sigma_T(T-T_0)$, where σ_T is assumed to be constant and positive. The fluids are considered to satisfy the Boussinesq approximation, i.e., the density variations caused by the thermal expansion are relatively small: $\beta\Delta T \ll 1$. In this case, the physical properties are independent of temperature, except density, which decreases with the local temperature: $\rho=\rho_0[1-\beta(T-T_0)]$, where β is the thermal expansion coefficient, ρ is the density, and ρ_0 is the density at the reference temperature T_0. After we introduce the vibration, the complete acceleration item $\mathbf{a}$ in Boussinesq equations should include both the static gravity and the vibrational acceleration, which is express as $\mathbf{a}=\mathbf{g}+\mathbf{n}b\Omega^2\cos(\Omega t)$, where $\mathbf{n}=\cos\alpha\mathbf{e}_x+\sin\alpha\mathbf{e}_z$ is the unit vector along the orientation of vibration, α is the vibration angle, b is the amplitude of vibration, and Ω is the angular frequency.

The interface between the two fluids is a free surface located at $z=h(x,t)$, where the mean value of $h(x,t)$ is zero. However, free-surface deformation has a relatively small effect on the thermal instability. Pearson[12] first studied the Marangoni instability in a liquid film with a nondeformable interface. Until now, the nondeformable assumption has been widely used in many works on the Marangoni stability. We consider the limit of $S\to\infty$, in which the free surface becomes a planar, nondeformable interface.[13] Here, the nondimensional surface tension number S is defined as $S=\sigma L/\rho\nu^2$, in which σ is the surface tension and L is the character length. For the present problem, we are interested in the Rayleigh–Marangoni instability, in which the effect of interface deflexion is slight. So, in the present study, we assume that the interface between the two fluids is a nondeformable free surface.

Based on the Boussinesq approximation, the continuity, the Navier–Stokes, and the energy equations are

$$\nabla\cdot\mathbf{v}=0, \tag{1}$$

$$\frac{\partial\mathbf{v}}{\partial t}+\mathbf{v}\cdot\nabla\mathbf{v}=-\frac{\nabla p}{\rho_0}+\nu\Delta\mathbf{v}+g\beta T\mathbf{e}_z+\beta Tb\Omega^2\cos\Omega t\mathbf{n}, \tag{2}$$

$$\frac{\partial T}{\partial t}+\mathbf{v}\cdot\nabla T=\kappa\Delta T. \tag{3}$$

Here, $\mathbf{v}$ is the velocity vector, p is the pressure, g is the gravity, ν is the kinematic viscosity, and κ is the thermal diffusivity. The operator Δ is the Laplacian.

A. Averaged equation and boundary conditions

The existence of a vibrational force leads to the development of the convective flow component oscillating with time. Thus, the velocity, temperature, and pressure field may be presented as superpositions of a mean and pulsational parts,[9]

$$\mathbf{v}=\bar{\mathbf{v}}+\mathbf{v}',\quad T=\bar{T}+T',\quad p=\bar{p}+p'. \tag{4}$$

The physical system is characterized by five different timescales. While the viscous diffusion timescale $\tau_{\text{visc}}=L^2/\nu$ and the thermal diffusion timescale $\tau_{\text{th}}=L^2/\kappa$ are related to the dissipative properties of the fluid, the buoyant timescale $\tau_b=(L/\beta\Delta Tg)^{1/2}$ and the thermocapillary timescale $\tau_{\text{tc}}=(\rho L^3/\sigma_T\Delta T)^{1/2}$ characterize the driving force of the

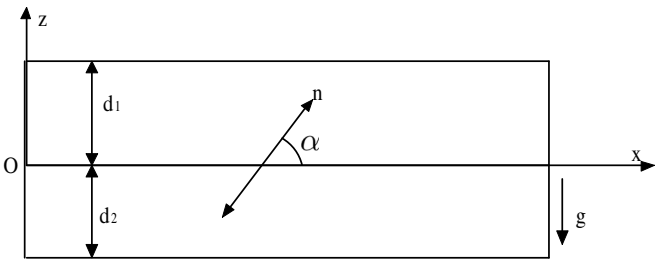

FIG. 2. A sketch of the physical model.

buoyancy and the surface tension, and the dynamic timescale $\tau_v = 1/\Omega$ is related to the vibration.

We assume that the frequency is high: $\tau_v \ll \tau_{\text{visc}}$, $\tau_{\text{th}}, \tau_b, \tau_{\text{tc}}$. The pulsational parts $\mathbf{v}', T', p'$ are assumed to oscillate quickly, with the reference time on the order of the vibration period τ_v. The average parts $(\bar{\mathbf{v}}, \bar{T}, \bar{p})$ are "slow" functions of time, responding to the dissipation process or the effects of buoyancy and thermocapillary. Substituting Eq. (4) into the controlling equations and selecting "fast" terms, we can obtain the equations for the oscillatory components,

$$\frac{\partial \mathbf{v}'}{\partial t} + (\bar{\mathbf{v}} \cdot \nabla)\mathbf{v}' + (\mathbf{v}' \cdot \nabla)\bar{\mathbf{v}} + (\mathbf{v}' \cdot \nabla)\mathbf{v}' = -\frac{\nabla p'}{\rho} + \nu \nabla^2 \mathbf{v}' + g\beta T' \mathbf{e}_z + \beta(\bar{T} + T')b\Omega^2 \cos \Omega t \mathbf{n}, \tag{5}$$

$$\frac{\partial T'}{\partial t} + (\bar{\mathbf{v}} \cdot \nabla)T' + \mathbf{v}' \nabla \bar{T} + \mathbf{v}' \nabla T' = \kappa \nabla^2 T'. \tag{6}$$

The assumption of $\tau_v \ll \tau_{\text{visc}}, \tau_{\text{th}}$ can be interpreted as small thicknesses of the boundary layers induced by vibrations are much less than the character length,

$$\delta_{\text{visc}} = \sqrt{\frac{\nu}{2\Omega}} \ll L, \quad \delta_{\text{th}} = \sqrt{\frac{\kappa}{2\Omega}} \ll L. \tag{7}$$

This assumption enables us to consider hydrodynamic fields in the bulk and in the boundary layer separately. Additionally, we assume that the amplitude of vibration is small: $b \ll L$. Based on these assumptions, all the terms including $\mathbf{v}'$ except for the leading term $\partial \mathbf{v}'/\partial t$ can be neglected in Eq. (5). In a similar way, all the terms including T' except for the leading term $\partial T'/\partial t$ can be neglected in Eq. (6). Among the terms describing convection oscillatory forces, the main one includes $\bar{T}$; we can simplify Eq. (5) further by retaining only the term that includes $\bar{T}$ and neglect the term that includes T'. We will defer the justification to the later part, after having the expressions for $\mathbf{v}'$ and T'. Following the standard procedure of the averaging method,[9] we present the vector $\bar{T}\mathbf{n}$ as the sum of solenoidal $\mathbf{w}$ and irrotational $\nabla\varphi$ parts,

$$\bar{T}\mathbf{n} = \mathbf{w} + \nabla\varphi. \tag{8}$$

We obtain that

$$\mathbf{v}' = \beta b\Omega \sin \Omega t \cdot \mathbf{w}, \tag{9}$$

$$T' = \beta b \cos \Omega t (\mathbf{w} \cdot \nabla \bar{T}). \tag{10}$$

From the expression of T', $T'/\bar{T}$ has the magnitude of $\beta \Delta T b/L$, which is much smaller than a unit. This result indicates that $\bar{T}$ is the main one that describes convection oscillatory forces, thus it is reasonable to neglect T' in the last term in Eq. (5). Comparing $g\beta T'$ with $\partial v'/\partial t$ and using the expressions of v' and T', the former can be neglected under the relationship between the gravity acceleration and the vibrational one,

$$\frac{g}{L\Omega^2}\beta \Delta T \ll 1. \tag{11}$$

This relationship is equivalent to the assumption that $\tau_v \ll \tau_b$.

Before we study the stability problem, let us now formulate the boundary conditions for the oscillatory velocity. Note that the viscous force driving the oscillatory flow has been neglected when deriving the pulsational equations. This means that the existence of the Stokes boundary layer for the pulsation flow is not taken into account.

On a rigid boundary, the no-slip condition for the velocity leads to the formation of a well-pronounced boundary layer. However, for a free surface of a fluid layer, the condition on the tangential stress contains only the velocity derivatives. This means that the boundary layer near the free surface is less pronounced and would manifest itself only in higher spatial derivatives of the velocity field. However, for the two-layer system, both the continuity of velocity and the balance of the tangential stresses should be satisfied at the interface between two fluids. If there is a difference between the bulk velocities of the two fluids, boundary layer should exist on each side of the interface. The magnitude of the boundary layer thickness is $\sqrt{\nu_1/2\Omega}$ or $\sqrt{\nu_2/2\Omega}$ on each side of the interface. In the high-frequency limit, the boundary layer is well-pronounced on the interface as well as on the rigid boundaries. Thus, the continuity of tangential velocity and the balance of tangential stress are not required on the boundaries. On the nondeformable interface, nonpermeability condition should be imposed rather than the nonslip one,

$$\mathbf{v}' \cdot \mathbf{n} = 0. \tag{12}$$

B. Spectral amplitude problem

We scale the problem by using d, d^2/ν_2, ν/d, and ΔT for length, time, velocity, and temperature. We assume that a mechanical quasiequilibrium exists and has the following structure:

$$T_{10} = T_{10}(z), \quad \mathbf{w}_{10} = [w_{10}(z), 0, 0], \tag{13}$$

$$T_{20} = T_{20}(z), \quad \mathbf{w}_{20} = [w_{20}(z), 0, 0]. \tag{14}$$

The nondimensional temperature gradients in the upper and lower layers are denoted by $-A_1$ and $-A_2$,

$$A_1 = \frac{1+h}{k^*+h}, \quad A_2 = \frac{k^*(1+h)}{k^*+h}. \tag{15}$$

Here, h is the depth ratio, which is defined as $h = d_1/d_2$.

For w_0, one has the nondimensional forms

$$\frac{dw_{10}}{dz} = -A_1 \cos \alpha, \tag{16}$$

$$\frac{dw_{20}}{dz} = -A_2 \cos \alpha. \tag{17}$$

Substituting Eqs. (9) and (10) into the complete set of equations and averaging them with respect to the fast time, we can obtain the equations for variables $\bar{\mathbf{v}}, \bar{p}, \bar{T}, \bar{w}$. We

introduce two-dimensional normal mode perturbations in the form as

$$(\bar{u},\bar{v},\bar{w}_z,\bar{p},\bar{T}) = [U(z),V(z),W(z),P(z),\Theta(z)] \times \exp[\lambda t + ikx], \tag{18}$$

where λ is the time growth rate and k is the wavenumber of the x direction. Eliminating the pressure $\bar{p}$ and the component $\bar{u}$, we get the normal mode equations,

$$\lambda \Delta V_1 = \nu^* \Delta\Delta V_1 - \frac{\beta^* \ \mathrm{Ra}}{\mathrm{Pr}} k^2 \Theta_1 + \frac{A_1 \varepsilon^* \ \mathrm{Ra}_v}{\mathrm{Pr}} \times (-k^2 \cos^2 \alpha\Theta_1 + ik \cos \alpha \mathrm{D} W_1 + k^2 \sin \alpha W_1), \tag{19}$$

$$\lambda \Theta_1 = A_1 V_1 + \frac{\kappa^*}{\mathrm{Pr}} \Delta \Theta_1, \tag{20}$$

$$\Delta W_1 = -ik \cos \alpha \mathrm{D}\Theta_1 - k^2 \sin \alpha \Theta_1, \tag{21}$$

$$\lambda \Delta V_2 = \nu^* \Delta\Delta V_2 - \frac{\mathrm{Ra}}{\mathrm{Pr}} k^2 \Theta_2 + \frac{A_2 \ \mathrm{Ra}_v}{\mathrm{Pr}} \times (-k^2 \cos^2 \alpha\Theta_2 + ik \cos \alpha \mathrm{D} W_2 + k^2 \sin \alpha W_2), \tag{22}$$

$$\lambda \Theta_2 = A_2 V_2 + \frac{\kappa^*}{\mathrm{Pr}} \Delta \Theta_2, \tag{23}$$

$$\Delta W_2 = -ik \cos \alpha \mathrm{D}\Theta_2 - k^2 \sin \alpha \Theta_2. \tag{24}$$

On the rigid boundary, the temperatures are assumed to be fixed, and the averaged velocity satisfies the no-slip condition. On the interface, the temperature and the heat flux are continuous, and the continuity of the averaged velocity and the balance of tangential stresses are satisfied. The oscillatory velocity satisfies the nonpermeability condition on both the rigid boundaries and the interface.

Boundary conditions at the bottom,

$$V_2 = \mathrm{D}V_2 = \Theta_2 = W_2 = 0, \tag{25}$$

at the top,

$$V_1 = \mathrm{D}V_1 = \Theta_1 = W_1 = 0, \tag{26}$$

and at the interface,

$$V_1 = V_2 = 0, \tag{27}$$

$$\mathrm{D}V_1 = \mathrm{D}V_2, \tag{28}$$

$$\Theta_1 = \Theta_2, \tag{29}$$

$$k^* \mathrm{D}\Theta_1 = \mathrm{D}\Theta_2, \tag{30}$$

$$(\mathrm{D}^2 + k^2)V_2 - \mu^*(\mathrm{D}^2 + k^2)V_1 = -k^2 \ \mathrm{Ma} \ \Theta_2, \tag{31}$$

$$W_1 = W_2 = 0. \tag{32}$$

Here, the operator D denotes differential operation $\mathrm{d}/\mathrm{d}z$ and Δ denotes $\mathrm{D}^2 - k^2$. The parameters include the Prandtl number (Pr), the Rayleigh number (Ra), the vibrational Rayleigh number (Ra_v), the Marangoni number (Ma), and the Bond number (Bo), which are defined as follows:

$$\mathrm{Pr} = \frac{\nu_2}{\kappa_2}, \quad \mathrm{Ra} = \frac{g\beta_2 \Delta T d^3}{\nu_2 \kappa_2}, \quad \mathrm{Ra}_v = \frac{\varepsilon_2 \Delta T^2 d^2}{\nu_2 \kappa_2}, \tag{33}$$

$$\mathrm{Ma} = \frac{\sigma_T \Delta T d}{\mu_2 \kappa_2}, \quad \mathrm{Bo} = \frac{\rho_2 g \beta_2 d^2}{\sigma_T}.$$

The ratios of physical properties include $\beta^* = \beta_1/\beta_2$, $\kappa^* = \kappa_1/\kappa_2$, $k^* = k_1/k_2$, $\mu^* = \mu_1/\mu_2$, $\nu^* = \nu_1/\nu_2$, and $\varepsilon^* = \varepsilon_1/\varepsilon_2$.

III. NUMERICAL METHOD

We transform the domains of $(0, d_1/d)$ and $(-d_2/d, 0)$ into the Chebyshev domain $(-1,1)$ by introducing $\zeta_1 = 2zd/d_1 - 1$ and $\zeta_2 = 2zd/d_2 + 1$. The variables $V_1, W_1, \Theta_1, V_2, W_2, \Theta_2$ are expanded using Chebyshev expansions

$$V_1 = \sum_{n=0}^{N} \hat{V}_1^n T_n(\zeta_1), \quad W_1 = \sum_{n=0}^{N} \hat{W}_1^n T_n(\zeta_1),$$

$$\Theta_1 = \sum_{n=0}^{N} \hat{\Theta}_1^n T_n(\zeta_1), \tag{34}$$

$$V_2 = \sum_{n=0}^{N} \hat{V}_2^n T_n(\zeta_2), \quad W_2 = \sum_{n=0}^{N} \hat{W}_2^n T_n(\zeta_2),$$

$$\Theta_2 = \sum_{n=0}^{N} \hat{\Theta}_2^n T_n(\zeta_2).$$

Equations (19)–(24), together with the corresponding boundary conditions, lead to a 16th order eigenvalue problem. We force expansion of Eq. (34) to satisfy the controlling equations and the boundary conditions at the Gauss–Lobatto points, the system of equations is required to solve for $6(N+1)$ unknowns of the spectral coefficients. This gives rise to an eigenvalue problem of the form

$$AX = \lambda BX \tag{35}$$

for eigenvalue λ, in which A and B are $6(N+1) \times 6(N+1)$ matrices, and the eigenvector X is the expansion coefficient in Eq. (34). The real part of the complex eigenvalue is the time growth rate and the imaginary part is the oscillatory frequency. In this paper, we denote the oscillatory frequency by ω. Details of the computational procedures can be found in Ref. 14. In the present paper, it is found that $N=20$ is enough to yield satisfactory results. We compute the most unstable eigenvalue for $k=4.6$, $h=1$, $\mathrm{Ra}_v=0$, and $\mathrm{Ra}=8181.0$. We obtain $\lambda = 4.76 \times 10^{-5}$, 0.11×10^{-4}, and 0.25×10^{-4} for $N=20$, 30, and 40, respectively. We also compute the critical Rayleigh number for $k=4.6$, $h=1$, and $\mathrm{Ra}_v=0$. The critical Rayleigh numbers are $\mathrm{Ra}=8381.4$, 8380.91, 8379.73 for $N=20$, 30, 40, respectively. The relative error $\Delta\mathrm{Ra}/\mathrm{Ra}$ is less than 10^{-4} for $N=20$. This result shows that $N=20$ yield almost indistinguishable critical value of Ra from $N=30,40$.

TABLE I. Physical properties of the two-layer system at 298 K.

	Property				
	ρ (kg/m^3)	β (1/K)	k (W/m K)	κ (m^2/s)	ν (m^2/s)
Silicone oil 10cs	953	1.1×10^{-3}	1.34×10^{-1}	9.50×10^{-8}	1.0×10^{-5}
FC70	1940	1.0×10^{-3}	6.99×10^{-2}	3.44×10^{-8}	1.4×10^{-5}

IV. RESULTS AND DISCUSSION

In this section, the instability characteristics of a real two-layer system will be investigated. Before we study the coupling mechanism of different instability modes and structures of the flow patterns, it is helpful to review the physics of different coupling modes that occur in the present system. In this paper, we limit our results to the instabilities of a system subjected to vertical and horizontal vibrations. In the system considered here, the upper fluid is silicone oil 10sc and the lower fluid is fluorinert FC70. The physical properties used in the calculations are listed in Table I. The total depth of the system is fixed at 6 mm and the Bond number is fixed at 15.35.

The Boussinesq approximation is valid for $\beta\Delta T \ll 1$. For the present problem, $\beta \sim 10^{-3}$ K^{-1}, so we could limit the $\Delta T \leq 10$ K. If the depth of the system is of the magnitude of 1 cm, this range of ΔT allows $|\mathrm{Ra}|$ to change from 0 to about 2.5×10^5. If we increase the depth d, a wider range of Ra is allowed without violating the Boussinesq approximation. The averaging method is valid upon the assumption of $\tau_\Omega \ll \tau_{\mathrm{visc}}, \tau_{\mathrm{th}}, \tau_b, \tau_{\mathrm{tc}}$. For $d \sim 1$ cm, we obtain that $\tau_{\mathrm{visc}} \sim 10$ and $\tau_{\mathrm{th}} \sim 10^3$. In the range of $\Delta T < 10$ K, $\tau_b > 0.32$ and $\tau_{\mathrm{tc}} > 1.3$. This conditions are satisfied if $1/\Omega \ll 1$. In the condition of $\Omega \gg 1$, the averaging method could be safely used.

For $d \sim 1$ cm and $\Delta T \sim 10$ K, $(b\Omega)^2 \approx 10$ corresponds to $\mathrm{Ra}_v \approx 10^5$. For a small $b \ll 10^{-3}$, the frequency Ω needs to have a magnitude $\gg 3\times10^3$ to reach such a high Ra_v. This is physically unrealistic for $d \sim 1$ cm. However, for other systems with larger depth d, a very large Ra_v is possible. In the present study, we note that the values of Ra_v are not intended to be physically realistic; rather, they allow us to characterize the influence of this parameter on the instability of the system, especially the instability characteristics for $\Omega \to \infty$.

A. Physics of different coupling modes

For a two-layer system heated from below, Johnson and Narayanan[15] presented five typical convection modes at different depth ratios. To understand the mechanisms of different instability modes, it is helpful to review the convection modes discussed in Ref. 15. At the onset of instability, in a thin fluid layer, surface tension driven convection (Marangoni convection) dominates, and in a thick fluid layer, buoyancy-driven convection (Rayleigh convection) dominates. We first neglect the surface tension and consider the case of Rayleigh convection. When the depth of the upper layer is much smaller than that of the lower layer, convection initiates in the lower layer and the upper layer is moved by the viscous drag of the lower layer. This convection mode is referred to as "lower dragging" mode. With the increase of the depth of the upper layer, the effect of buoyancy becomes comparable in both layers. In this case, two convection modes are possible. One is "viscous coupling" mode, the other is that "thermal coupling" mode. The convection of "upper dragging," lower dragging, or viscous coupling is "mechanical coupling" mode. We should note that thermal coupling Rayleigh convection is a rare event and mechanical coupling is usually preferred.[3] For a system heated from below, the mechanical coupling mode is characterized by the rolls in each fluid layer rotating in the opposite directions, and the thermal coupling mode by the rolls in each layer rotating in the same direction. When the depth of the upper layer is larger than that of the lower layer, convection initiates in the upper layer because the buoyancy is dominant in the upper layer, and the lower layer is viscously dragged.

In the presence of the surface tension, a convection mode referred to as "pure thermal coupling with surface-driven flow" can occur. In Ref. 15, the flow pattern of pure thermal coupling with surface-driven flow is presented for a system heated from below. We present the schematic of this mode in Fig. 1(a). This convection mode typically occurs in a gas-liquid system, in which convection initiates in the upper layer, simultaneously sending thermal signature to the interface, and generating Marangoni convection or Rayleigh convection in the lower layer.[15] It seems that the flow pattern of the surface-driven flow is similar to that of thermal coupling mode without Marangoni effect, in which the rolls corotate in each layer.

In the absence of vibrations, Rayleigh–Marangoni convection only occurs in a system heated from below. There is no problem to distinguish the viscous coupling mode and the thermal coupling mode by identifying the directions of rotation of fluids. In these two cases, fluids corotate and counterrotate in each layer, respectively. However, when a system is cooled from below, identifying the directions of fluids is not enough to distinguish different coupling modes.

When the system is subjected to vibrations, Rayleigh–Marangoni convection may occur even when the system is cooled from below. To understand the mechanisms of convection in a system under vibrations, it is helpful to look at the flow patterns of the system heated and cooled from below. In Fig. 1(a), convection initiates in the upper layer in a liquid-liquid system heated from below, and the flow pattern is similar to that of a gas-liquid system in Ref. 15. In this figure, the flows in the upper layer send thermal signature to the interface and generate Marangoni convection in the lower layer. The interfacial flow and the Rayleigh convection in the

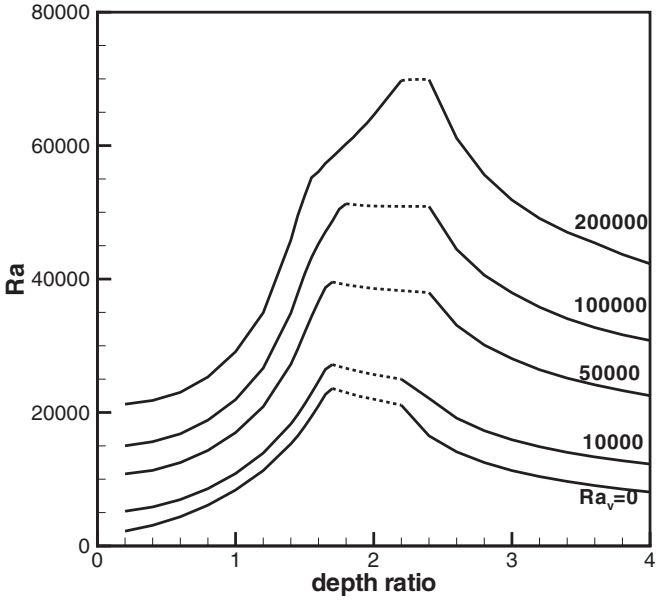

FIG. 3. The critical Rayleigh number vs depth ratio for various vibrational Rayleigh numbers. The oscillatory branches are denoted by dotted lines. The other parameters are $d=6$ mm, Bo=15.35, and vibration angel $\alpha=\pi/2$.

upper layer discourage each other. In Fig. 1(b), the flow pattern of convection initiating in the lower layer in a system heated from below is presented. In this figure, the rolls counter-rotate in each layer, and the interfacial flow and the Rayleigh convection enhance each other in the lower layer.

In Fig. 1(c), the flow pattern of convection initiating in the upper layer is presented for a system cooled from below. In this figure, the rolls counter-rotate in each layer, which is significantly different to the flow pattern in Fig. 1(a) for a system heated from below. In this figure, the interfacial flow and the convection in the upper layer enhance each other. In Fig. 1(d) for convection initiating in the lower layer in a system cooled from below, the rolls corotate in each layer. In this figure, the interfacial flow and the convection in the lower layer discourage each other.

In Fig. 1, we only give qualitative plots of convective modes under the assumption that convection initiates in either the upper layer or the lower layer. However, these plots do not include all situations. In experiments or computations, oscillatory convection may occur. In this paper, we can see that oscillatory convection is different from any case in Fig. 1. However, oscillatory convection is the result of the competition of different modes in Fig. 1.

B. Instabilities under vertical vibrations

We begin with the influences of vertical vibrations on the stability characteristics and the structures of flow patterns. Figure 3 presents the curves of the critical Rayleigh number versus the depth ratio for various vibrational Rayleigh numbers. It is shown that at a given Ra_v, each curve displays a trimodal structure. The left and right branches of the curves are the regions where convection initiates in the lower and upper layers, respectively. The dotted lines between the left and the right branches are the regions where oscillatory convection occurs. At the onset of instability, for each Ra_v, the time growth rate $\lambda=0$ in the left and right branches and $\lambda=\pm i\omega$ in the oscillatory branches. This result indicates that at the left and right branches, the convection is in the form of static rolls, and at the oscillatory branch, the convection is in the form of two traveling waves. In Fig. 3, all the critical Rayleigh numbers are positive. This means that convection occurs only when the system is heated from below. The structures of the flow patterns of the right and left branches are qualitatively shown in Figs. 1(a) and 1(b). In Figs. 1(a) and 1(b), it is assumed that the convection initiates in either the upper layer or the lower layer. However, when the Rayleigh effects in the upper and lower layers are comparable, the competition between different modes may occur. The oscillatory behavior is the result of the competition of different convective modes, i.e., convection initiating in the upper and lower layers. In Fig. 3, it is shown that the critical Rayleigh number significantly increases with the increase of the vibrational Rayleigh number at all depth ratios. Gershuni and Lyubinov[9] studied the interaction of the influence of the vibrational Rayleigh number on the critical Rayleigh number for a one-layer system. It is shown that the increase of Ra_v stabilizes the system. For pure Marangoni stability in a one-layer system, the increase of Ra_v also stabilizes the system.[16] It seems that in a two-layer system, the increase of Ra_v has the same effect as that in a one-layer system for both the Rayleigh stability and the Marangoni stability.

In order to know the effects of vibrations on the instabilities of different convection modes, we present the marginal curves of Rayleigh number versus the wavenumber with various vibrational Rayleigh numbers for several typical depth ratios. In Fig. 4(a), the marginal curves are presented for the depth ratio $h=1$, at which convection initiates in the lower layer at the onset of instability. In this figure, all the curves are unimodal. With the increase of the vibrational Rayleigh number, the system becomes more stable and the critical wavenumber decreases. As shown in Fig. 3, at the onset of instability, the oscillatory convection is the dominant mode at $\mathrm{Ra}_v=0$ for $h=2$. In Fig. 4(b) for the depth ratio $h=2$, each marginal curve displays a bimodal structure. The left branches of the curves are of the oscillatory mode, and the right branches are of the mode of convection initiating in the upper layer. In this figure, it is shown that with the increase of the vibrational Rayleigh number, both the left and the right branches become more stable. At $\mathrm{Ra}_v=0$, the oscillatory mode is the dominant; however, as Ra_v increase to 20 000, the dominant mode switches from the left branch to the right branch. As the depth ratio h increases to 2.3, as shown in Fig. 4(c), the curves for various Ra_v display a trimodal structure. In Fig. 3, at $\mathrm{Ra}_v=0$ for $h=2.3$, the dominant mode is the convection initiating in the upper layer, which corresponds to the left branch in Fig. 4(c). With the increase of Ra_v, all branches become more stable. As Ra_v increases to 10 000, the middle branch and the left branch become almost the same stable. As Ra_v increases further, the middle branch becomes the dominant mode. As the depth ratio h increases to 3, all the curves in Fig. 4(d) also display a trimodal structure. With the increase of Ra_v, all branches become more stable; however, the dominant mode is always located in the left branch.

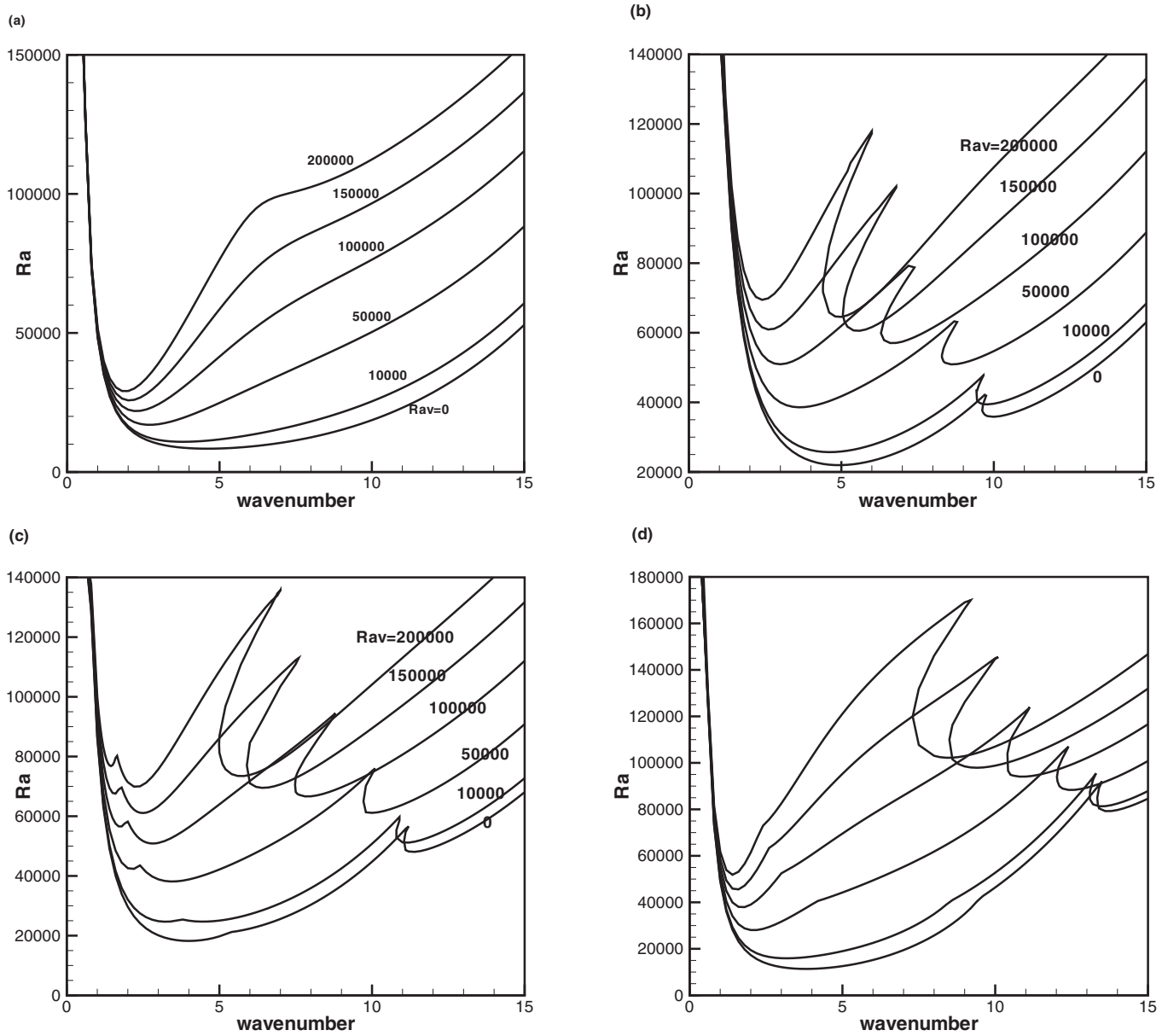

FIG. 4. The marginal curves of the Rayleigh number vs the wavenumber with various vibrational Rayleigh numbers for different depth ratios: (a) $h=1.0$, (b) $h=2.0$, (c) $h=2.3$, and (d) $h=3.0$. The other parameters are $d=6$ mm, Bo=15.35, and $\alpha=\pi/2$.

In order to know the physics of different convective modes, we will present the structures of the flow patterns for several typical cases. In each case, the flow patterns of streamlines, the isolines of the temperature disturbances, and the amplitudes of V and Θ are presented. In the plots of streamlines, the solid lines denote the rolls rotating anticlockwise, and the dashed lines denote the rolls rotating clockwise. In the plots of isolines of temperature disturbances, the solid and the dashed lines denote positive and negative disturbances, respectively. In the plots of the amplitudes of V and Θ, the real parts are denoted by solid lines and the imaginary parts are denoted by dashed lines.

In Fig. 5, the flow patterns and the amplitudes of V and Θ are presented for $h=1$ at $\mathrm{Ra}_v=200\,000$ at the onset of instability. The corresponding marginal curve is shown in Fig. 4(a). When convection initiates in the lower layer, the upper layer can be viscously dragged or driven by surface tension. In this case, the surface-driven flow is qualitatively depicted in Fig. 1(b). In Fig. 5(a), the surface-driven flow and the viscously dragged flow reinforce each other in the upper layer, and the rolls counter-rotate in each layer. The convection patterns in Fig. 5(a) are similar to the viscous coupling mode in Ref. 15. In this case, identifying the direction of flow could not distinguish the viscous coupling mode and the thermal coupling mode. In order to know more about the characteristics of different coupling modes, it is helpful to look at the temperature disturbances. In Fig. 5(c), it is shown that the patterns of the isothermal lines mainly locate in the lower layer. Figure 5(d) shows that the amplitudes of temperature disturbances in the lower layer are larger than that in the upper layer. This result is consistent with the fact that the convection initiates in the lower layer. Strictly speaking, if the convection in the upper layer is completely a passive response to the convection initiating in the lower layer,

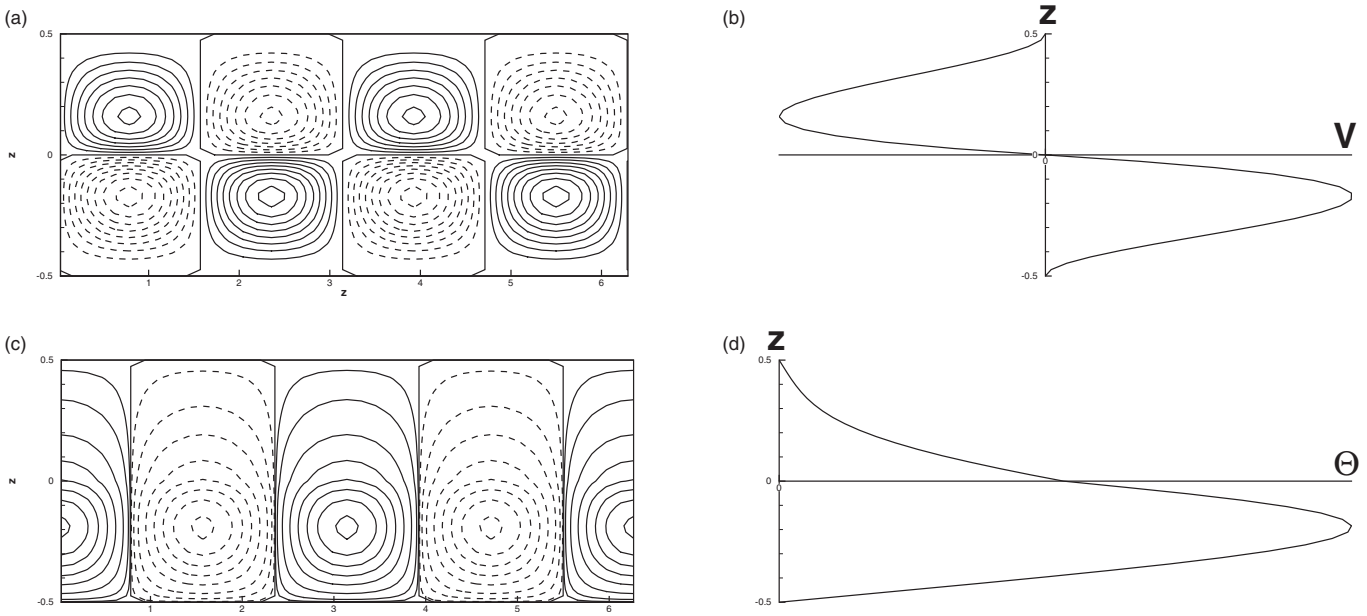

FIG. 5. Plots of the flow patterns and the amplitudes of V and Θ at the onset of convection: (a) streamline patterns, (b) amplitude of V, (c) contours of the temperature disturbances, and (d) amplitude of Θ. The other parameters are $h=1.0$, $\mathrm{Ra}_v=200\,000$, $\mathrm{Bo}=15.35$, $d=6$ mm, $k=2.0$, and $\mathrm{Ra}=29\,112.9$.

the magnitude of the velocity component V should be much lower in the upper layer than that in the lower layer. We should note that for $h=1$, the Rayleigh effect is comparable in each layer, and moreover, the Marangoni effect and viscous coupling reinforce in the upper layer. Consequently, the magnitudes of V in different layers are comparable. Fixing other parameters and only changing the vibrational Rayleigh number, we found that the structures of the flow patterns are qualitatively the same as that in Fig. 5.

In Fig. 6, the flow patterns and the amplitudes of V and Θ are presented for $h=2$ at $\mathrm{Ra}_v=100\,000$. In Fig. 6(a), it is shown the flow patterns of streamlines tilt to the left. However, in Fig. 6(c), the patterns of the temperature disturbances tilt to the right. In Figs. 6(b) and 6(d), the amplitudes of V and Θ are complex functions of z. The real part of V has a different sign in each layer. The imaginary part of V has the same sign in each layer; however, the magnitude of the imaginary part of V in the lower layer is much smaller than that in the upper layer. Figure 6(d) shows that the imaginary part and real parts of Θ correspond to convection initiating in the upper and lower layers, respectively. It seems that the imaginary and real parts of the amplitudes of V and Θ cor-

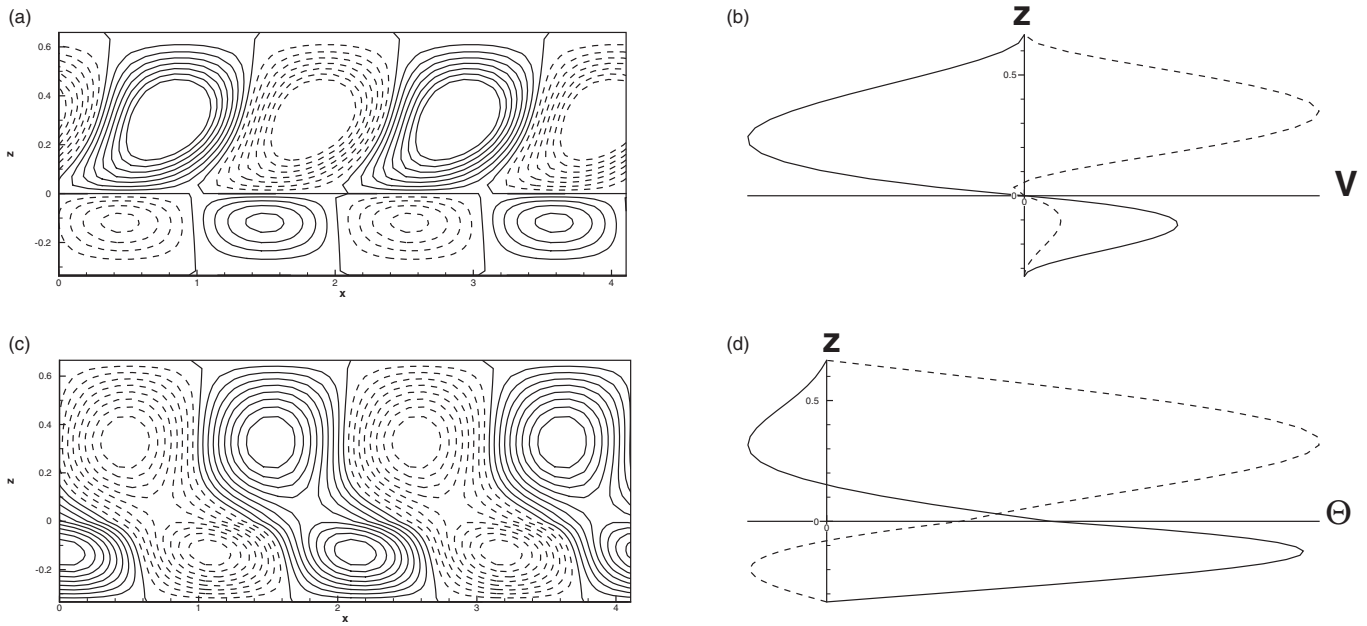

FIG. 6. Plots of the flow patterns and the amplitudes of V and Θ for the left traveling wave at the onset of convection: (a) streamline patterns, (b) amplitude of the vertical component, (c) temperature contour, and (d) amplitude of the temperature. The other parameters are $h=2.0$, $\mathrm{Ra}_v=100\,000$, $\mathrm{Bo}=15.35$, $d=6$ mm, $k=3.0$, and $\mathrm{Ra}=50\,942.3$. The frequencies of the two traveling waves are $\omega=\pm 0.1083$.

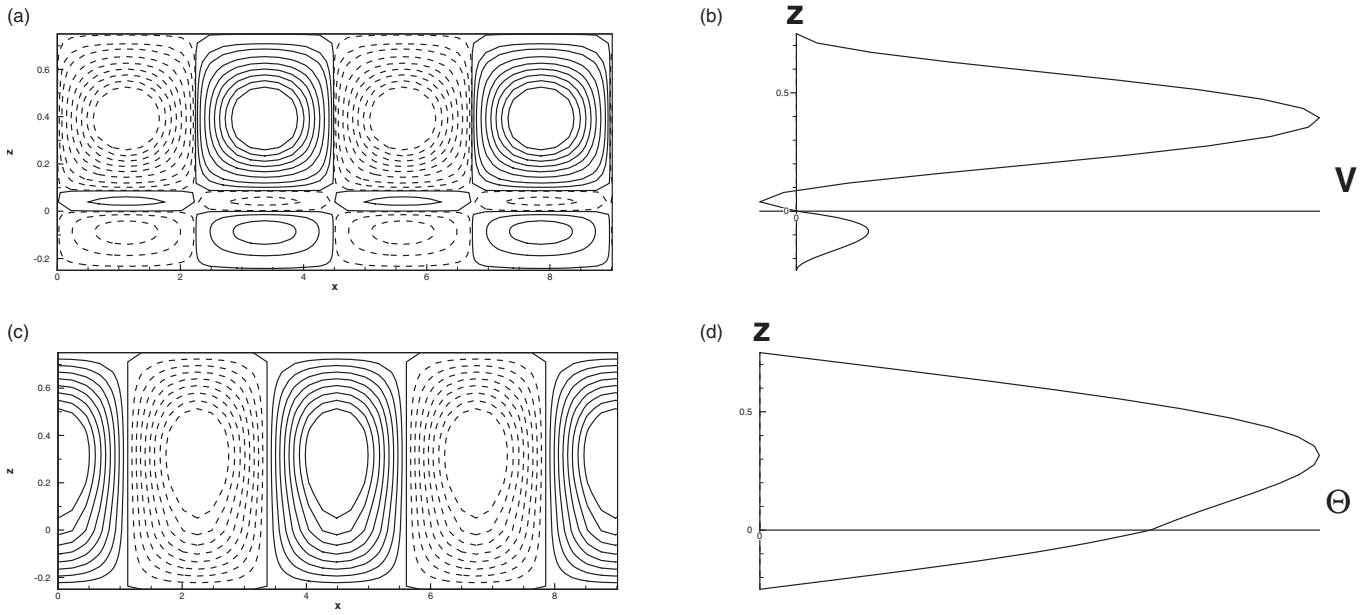

FIG. 7. Plots of the flow patterns and the amplitudes of V and Θ at the onset of convection: (a) streamline patterns, (b) amplitude of V, (c) contours of the temperature disturbances, and (d) amplitude of Θ. The other parameters are $h=3.0$, $\mathrm{Ra}_v=200\,000$, $\mathrm{Bo}=15.35$, $d=6$ mm, $k=1.4$, and $\mathrm{Ra}=51\,849.5$.

respond to the convection initiating in the upper and lower layers, respectively. The oscillatory convection is the result of the alternation between these two modes.

For $h=3$, the dominant mode is convection initiating in the upper layer. Figure 7 presents the flow patterns and the amplitudes of V and Θ at $\mathrm{Ra}_v=200\,000$. The structures of the main flow in Fig. 7(a) are qualitatively the same as that in Fig. 1(a). In Fig. 7(a), the magnitude of V is much smaller in the lower layer than that in the upper layer, and the rolls corotate in each layer. Figure 7(d) shows that the maximum temperature disturbance is located in the lower layer. This result indicates that convection initiates in the upper layer and the flow in the lower layer is driven by the surface tension. In Fig. 7(a), it is found that a series of weak counter-rolls has developed in the upper layer near the interface. In order to know the mechanism of the presence of these counter-rolls, it is helpful to return to Fig. 1(a). As shown in this figure, the direction of the interfacial flow is opposite to the convection flow in the upper layer. Consequently, a series of counter-roll is generated by the shear force between the interfacial flow and the upper flow to preserve the no-slip condition between the fluids.

C. Instabilities under horizontal vibrations

In this subsection, we will investigate the influences of horizontal vibrations on the stability of the system. Figure 8 presents the curves of the critical Rayleigh number versus the depth ratio for various vibrational Rayleigh numbers when the system is subjected to horizontal vibrations. As shown in this figure, the critical Rayleigh number decreases with the increase of Ra_v at all depth ratios. Fixing the depth ratio, some critical Rayleigh numbers become negative as Ra_v increases to a certain value. This result indicates that in the presence of horizontal vibrations, the system can become unstable even though it is cooled from below. For $\mathrm{Ra}_v=0$, 10 000, 20 000, and 50 000, it is obvious that there is an oscillatory region in each curve. For $\mathrm{Ra}_v=0$, 10 000, and 20 000, the critical Rayleigh numbers of the oscillatory regions are positive. When the critical Rayleigh number is positive, the increase of Ra_v narrows the oscillatory region. As Ra_v increases to 30 000, the critical Rayleigh number at the peak of the curve approximates to zero. At the onset of instability corresponding to this peak, the temperature difference ΔT is slight. In this case, the Marangoni effect at the interface is very weak, thus the competition between the left

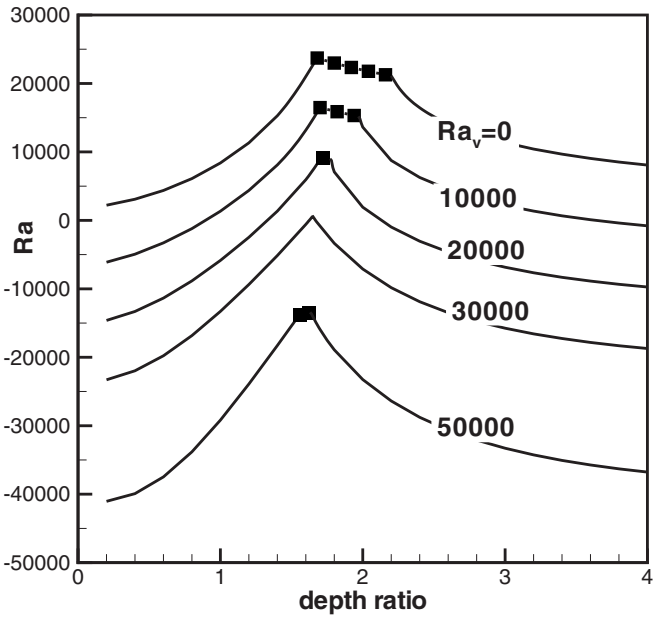

FIG. 8. The critical Rayleigh number vs depth ratio for various vibrational Rayleigh numbers. The oscillatory regions are labeled by squares. The other parameters for the system are $d=6$ mm, $\mathrm{Bo}=15.35$, and vibration angel $\alpha=0$.

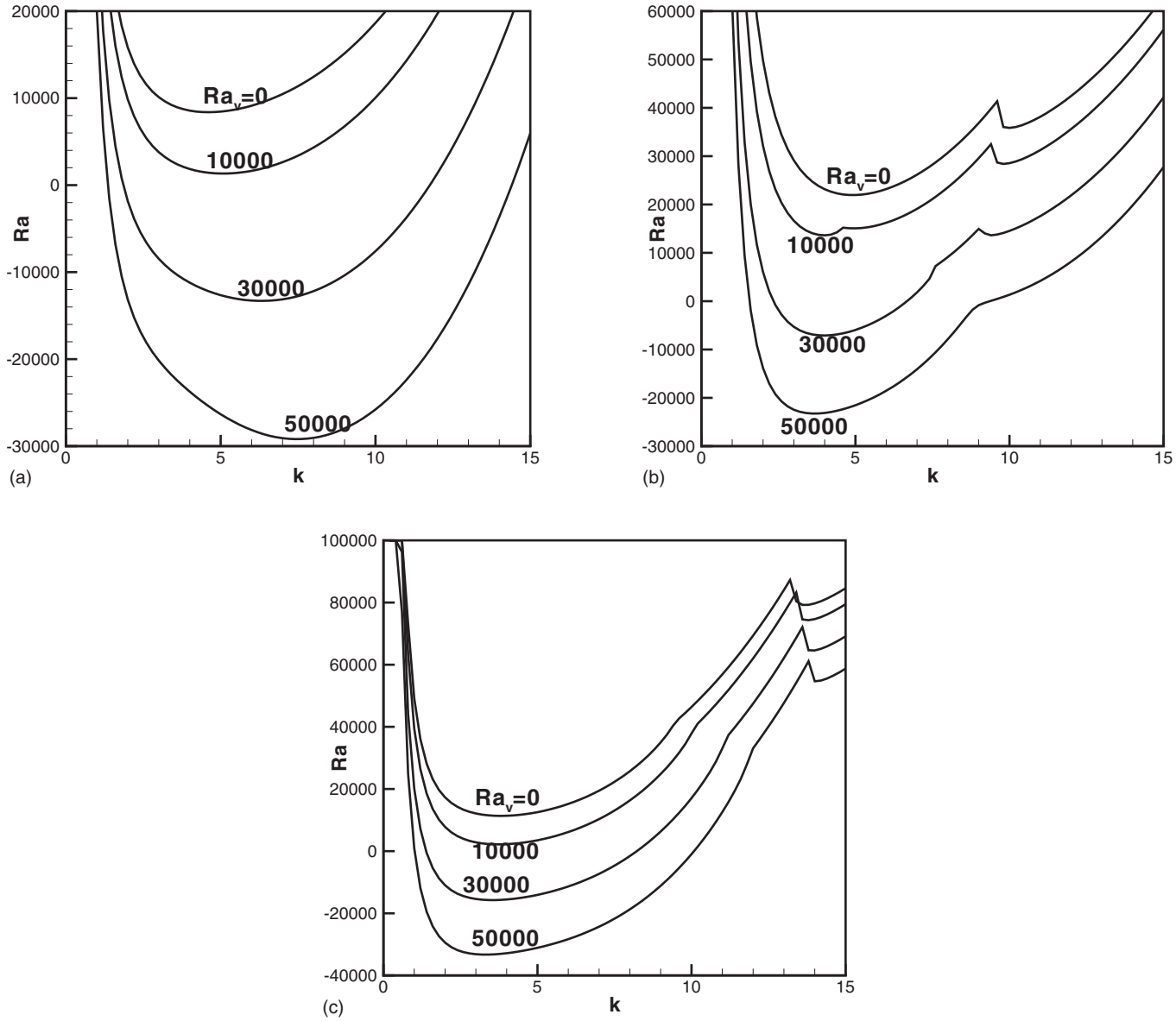

FIG. 9. The marginal curves of the Rayleigh number vs the wavenumber with various vibrational Rayleigh numbers for different depth ratios: (a) $h=1.0$, (b) $h=2.0$, and (c) $h=3.0$. The other parameters are $d=6$ mm, Bo=15.35, and $\alpha=0$.

branch and the right branch is almost impossible. This is the reason that the oscillatory branch nearly disappears in the curve of $\mathrm{Ra}_v=30\,000$. As Ra_v increases more, the critical Rayleigh number becomes negative. At the onset of instability, the magnitude of the temperature difference in the combined layers is nonzero. Thus, the Marangoni effect will play a role in the competition of different modes, and the oscillatory region reappears in the curve of $\mathrm{Ra}_v=50\,000$. From the above discussion, the horizontal vibration will destabilize the system. In Fig. 8, it seems that when the critical Rayleigh numbers in the oscillatory region are positive, the increase of Ra_v narrows the oscillatory region; when the critical Rayleigh numbers in the oscillatory region are negative, the increase of Ra_v broadens the oscillatory region; and when the maximum critical Rayleigh number of the curve is zero, the oscillatory region disappears.

In order to know more about the effects of horizontal vibrations on the stability of different convection modes, Fig. 9 presents the marginal curves of the Rayleigh number versus the wavenumber for several typical cases. As shown in Fig. 9(a) for $h=1$, the marginal curves for all Ra_v display a unimodal structure. At all wavenumbers, the Rayleigh number decreases with the increase of Ra_v. As Ra_v decreases to 30 000, it is obvious that the critical Rayleigh number has become negative. As shown in Fig. 9(b) for $h=2$, the marginal curve of $\mathrm{Ra}_v=0$ is bimodal. The left branch corresponds to oscillatory mode, and the right branch corresponds to convection initiating in the lower layer. At $\mathrm{Ra}_v=0$, the oscillatory mode occurs at the onset of instability. As Ra_v increases to 10 000, a new left branch gradually appears and the convection initiating in the upper layer becomes the dominant mode. As Ra_v increases further, the left branch decreases more than the middle and right branches. As Ra_v increases to 50 000, the middle branch is completely suppressed by the left branch. Figure 9(c) presents the marginal curves for $h=3$. In this figure, each curve displays a trimodal

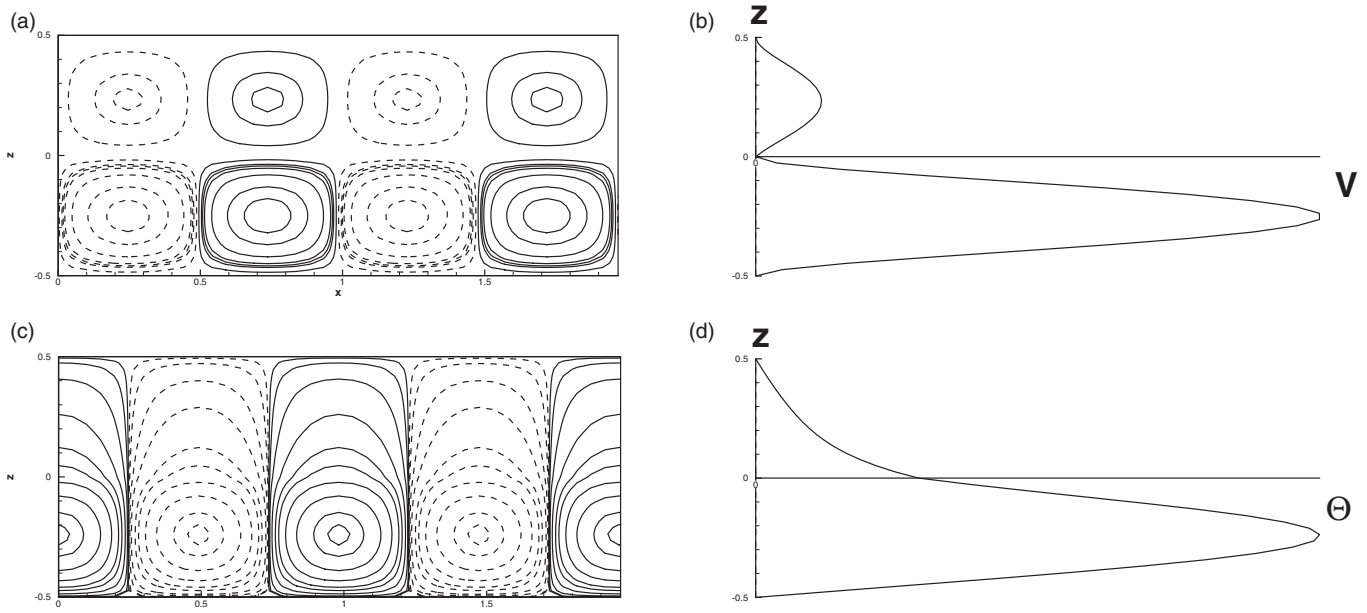

FIG. 10. Plots of the flow patterns and the amplitudes of V and Θ at the onset of convection: (a) streamline patterns, (b) amplitude of V, (c) contours of the temperature disturbances, and (d) amplitude of Θ. The other parameters are $h=1.0$, $\mathrm{Ra}_v=30\,000$, $\mathrm{Bo}=15.35$ $d=6$ mm, $\alpha=0$, $k=6.4$, and $\mathrm{Ra}=-13\,299.9$.

structure. With the increase of Ra_v, all branches become more unstable. However, the left branch is always the dominant mode.

In Fig. 10 for $h=1$ and $\mathrm{Ra}_v=30\,000$, at the onset of instability the critical Rayleigh number is negative. In Figs. 10(c) and 10(d), the patterns of the temperature disturbances and the amplitude of Θ indicate that the maximal temperature disturbances occur in the lower layer. In Figs. 10(a) and 10(b), the amplitude of V is much larger in the lower layer than that in the upper layer. It is obvious that the convection initiates in the lower layer, and the upper layer is driven by the surface tension. The flow pattern in Fig. 10(a) is qualitatively the same as that in Fig. 1(d). Being significantly different from that in Fig. 5(a) for vertical vibrations where rolls counter-rotate in each layer, in Fig. 10(a) the rolls corotate in each layer. As Ra_v increase to 50 000, the main flow patterns are similar to that in Fig. 10. However, we found that at the interface, a series of weakly counter-rolls has developed in the lower layer to preserve the no-slip condition between the fluids.

For $h=3$ at $\mathrm{Ra}_v=30\,000$, the critical Rayleigh number decreases to be a negative number. At the onset of convection, a large temperature difference exists in the combined layers, thus the Marangoni effect is dominant at the interface.

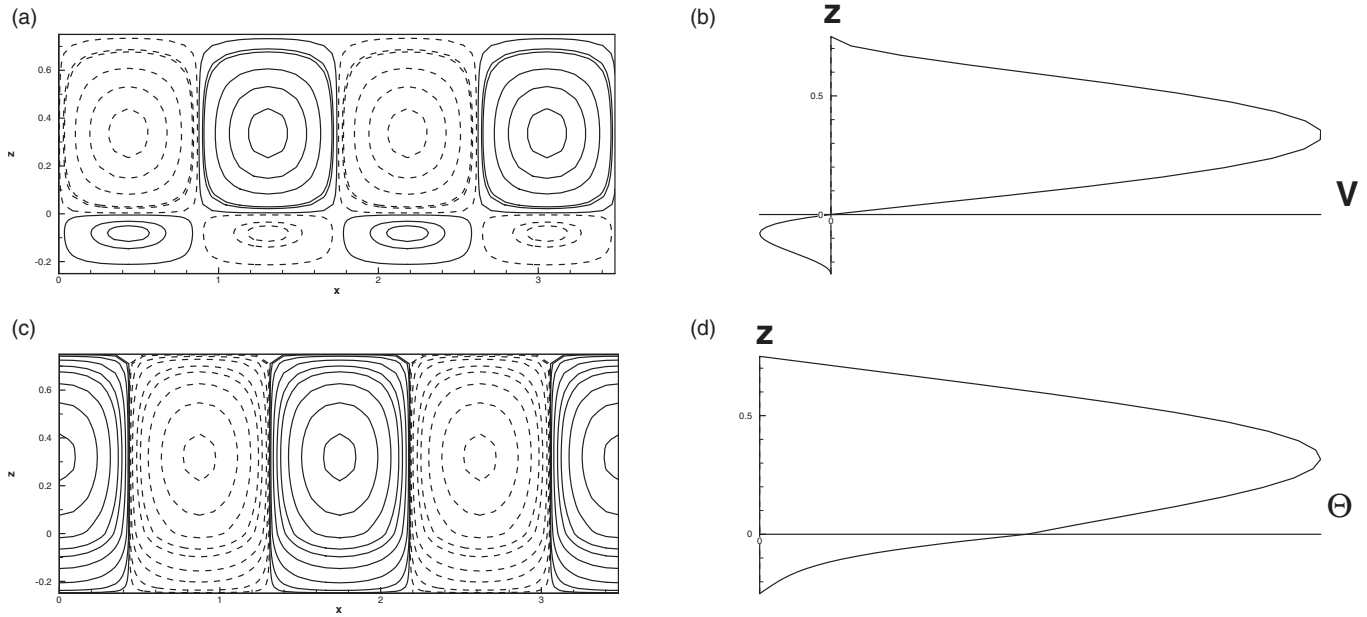

FIG. 11. Plots of the flow patterns and the amplitudes of V and Θ at the onset of convection: (a) streamline patterns, (b) amplitude of V, (c) contours of the temperature disturbances, and (d) amplitude of Θ. The other parameters are $h=3.0$, $\mathrm{Ra}_v=30\,000$, $\mathrm{Bo}=15.35$ $d=6$ mm, $\alpha=0$, $k=3.6$, and $\mathrm{Ra}=-15\,755.7$.

We note that in this case the Marangoni effect and the viscously coupling mode reinforce at the interface. The convection mode is qualitatively plotted in Fig. 1(c). In Fig. 11, the flow patterns and the amplitudes of V and Θ are presented for $h=3$ at $\mathrm{Ra}_v=30\,000$. In Fig. 11(b), the amplitude of V changes sign from the upper layer to the lower layer, and the magnitude of V in the lower layer is much smaller than that in the upper layer. Being similar to that in Fig. 7 for vertical vibrations, the convection in Fig. 11 initiates in the upper layer. In Figs. 11(c) and 11(d), the patterns of temperature disturbances and amplitude of Θ are very similar to that in Figs. 7(c) and 7(d). However, being different from that in Fig. 7, the rolls in Fig. 11(a) counter-rotate in each layer.

V. CONCLUSIONS

In the present paper, we have studied the effects of high-frequency vibrations on the Rayleigh–Marangoni instability in a two-layer system. Our results have shown that the depth ratio h plays an important role in determining the instability modes at the onset of convection.

In the absence of vibrations, convection initiates in the lower layer for small depth ratio and in the upper layer for large depth ratio. When the system is heated from below and Marangoni effect is dominant at the interface, the rolls counter-rotate in each layer for small h, whereas the rolls corotate in each layer for large h. Because these two modes of convection discourage each other, for a medium h, the two modes compete against each other, resulting in oscillatory convection.

The vibration angle α is a crucial parameter that influences the stability of the system. In the present paper, we limit our attention to two typical cases, i.e., vertical vibration ($\alpha=\pi/2$) and horizontal vibration ($\alpha=0$).

At $\alpha=\pi/2$, with the increase of Ra_v, the critical Rayleigh number significantly increases at all depth ratios. We have presented the marginal curves of the Rayleigh number versus the wavenumber for several depth ratios with various Ra_v. The structures of the marginal curves may display a trimodal structure. The branch of convection initiating in the upper layer is located on the left of the oscillatory branch, and the branch of convection initiating in the lower layer is located on the right of the oscillatory branch. It is shown that all the branches of marginal curves become more stable with the increase of the vibrational Rayleigh number. Fixing the wavenumber, the increase of Ra_v only influences the critical value of the Rayleigh number; however, it does not influence the direction of the rolls in each layer.

At $\alpha=0$, with the increase of Ra_v, all the branches become more unstable. In the presence of horizontal vibrations, instability may occur even though the system is cooled from below. The results show that when the critical Rayleigh number change from positive to negative, a stationary counter-rotating rolls will become a stationary corotating rolls at small h, and a stationary corotating rolls will become a stationary counter-rotating rolls at large h. Thus, for a system subjected to high-frequency vibrations, the surface-driven flows have four typical flow patterns, as shown qualitatively in Fig. 1. Our result shows that the oscillatory convection can be suppressed or even be completely eliminated by changing the vibrational Rayleigh number.

We have also made a tentative study on the structures of the interfacial flows. For some parameters, the surface flow induced by Marangoni effect and the convection in the initiating layer discourage each other. In these cases, a counter-roll will develop to preserve the nonslip condition in the layer where convection initiates.

ACKNOWLEDGMENTS

The authors thank the financial support for this research from the National Foundation of China (Grant Nos. 50890182, 11072249, and 10772185) and the Knowledge Innovation Program of Chinese Academy of Sciences (Grant No. KGCX-SW-409).

[1] Y. Renardy and D. Joseph, "Oscillatory instability in a Bénard problem of two fluids," Phys. Fluids **28**, 788 (1985).
[2] Y. Renardy and M. Renardy, "Perturbation analysis of steady and oscillatory onset in a Bénard problem with two similar liquids," Phys. Fluids **28**, 2699 (1985).
[3] S. Rasenat, F. H. Busse, and I. Rehberg, "A theoretical and experimental study of double-layer convection," J. Fluid Mech. **199**, 519 (1989).
[4] P. Colinet and J. C. Legros, "On the Hopf bifurcation occurring in the two-layer Rayleigh-Bénard convection instability," Phys. Fluids **6**, 2631 (1994).
[5] M. Le Bars and A. Davaille, "Stability of thermal convection in two superimposed miscible viscous fluids," J. Fluid Mech. **471**, 339 (2002).
[6] A. A. Nepomnyashchy and I. B. Simanovskii, "Influence of thermocapillary effect and interfacial heat release on convective oscillations in a two-layer system," Phys. Fluids **16**, 1127 (2004).
[7] Q. S. Liu, B. H. Zhou, T. H. Nguyen, and W. R. Hu, "Instability of two-layer Rayleigh-Benard convection with interfacial thermocapillary effect," Chin. Phys. Lett. **21**, 686 (2004).
[8] Q. S. Liu, B. H. Zhou, and Z. M. Tang, "Oscillatory instability of Rayleigh-Marangoni-Bénard convection in two-layer liquid systems," J. Non-Equilib. Thermodyn. **30**, 305 (2005).
[9] G. Z. Gershuni and D. V. Lyubimov, *Thermal Vibrational Convection* (Wiley, Chichester, 1998).
[10] Q. S. Liu, J. Y. Zhou, A. Wang, V. I. Polezhaev, A. Fedyushkin, B. H. Zhou, N. T. Henri, and B. Bernard, "Thermovibrational instability of Rayleigh Marangoni Bénard convection in two-layer fluid systems," J. Adv. Space Res. **41**, 2131 (2008).
[11] S. M. Zen'kovskaya and V. A. Novosyadlyi, "The effect of a high-frequency progressive vibration on the convective instability of a two-layer fluid," J. Appl. Math. Mech. **73**, 271 (2009).
[12] J. R. A. Pearson, "On convection cells induced by surface tension," J. Fluid Mech. **4**, 489 (1958).
[13] M. K. Smith and S. H. Davis, "Instabilities of dynamic thermocapillary liquid layers. Part 1. Convective instabilities," J. Fluid Mech. **132**, 119 (1983).
[14] C. Canuto, M. Y. Hussaini, A. Quarteroni, and T. A. Zang, *Spectral Methods in Fluid Dynamics* (Springer-Verlag, New York, 1988).
[15] D. Johnson and R. Narayanan, "Geometric effects on convective coupling and interfacial structures in bilayer convection," Phys. Rev. E **56**, 5462 (1997).
[16] S. M. Zen'kovskaya and A. L. Shleikel, "The effect of high-frequency vibration on the onset of Marangoni convection in a horizontal liquid layer," J. Appl. Math. Mech. **66**, 559 (2002).